Title: Synthesis and Characterisation of Cobalt Ferrite Coatings for Oxygen Evolution Reaction

Author: Julian Kubisztal, Marian Kubisztal

Citation style: Kubisztal Julian, Kubisztal Marian. (2022). Synthesis and Characterisation of Cobalt Ferrite Coatings for Oxygen Evolution Reaction. „Catalysts” (Vol. 11, iss. 1, 2022, art. no. 21, s. 1-11), DOI: 10.3390/catal12010021

catalysts

MDPI

Article

Synthesis and Characterisation of Cobalt Ferrite Coatings for Oxygen Evolution Reaction

Julian Kubisztal * and Marian Kubisztal

Institute of Materials Engineering, University of Silesia in Katowice, 75 Pułku Piechoty 1A, 41-500 Chorzow, Poland; marian.kubisztal@us.edu.pl

* Correspondence: julian.kubisztal@us.edu.pl; Tel.: +48-3-2349-7527

Abstract: In this paper, two novel procedures based on powder sedimentation, thermal treatment, and galvanostatic deposition were proposed for the preparation of porous cobalt ferrite ($CoFe_2O_4$) coatings with a metallic and organic binder for use as catalysts in the oxygen evolution reaction (OER). The electrochemical properties of the obtained electrode materials were determined as well, using both *dc* and *ac* methods. It was found that cobalt ferrite coatings show excellent electrocatalytic properties towards the oxygen evolution reaction (OER) with overpotential measured at a current density of 10 $mAcm^{-2}$ from 287 to 295 mV and a Tafel slope of 35–45 $mVdec^{-1}$. It was shown that the increase in the apparent activity of the $CoFe_2O_4$ coatings with an organic binder results mainly from a large electrochemically active area. Incorporation of the nickel binder between the $CoFe_2O_4$ particles causes an increase in both the conductivity and the electrochemically active area. The Tafel slopes indicate that the same rate-determining step controls the OER for all obtained coatings. Furthermore, it was shown that the $CoFe_2O_4$ electrodes exhibit no significant activity decrease after 28 h of oxygen evolution. The proposed coating preparation procedures open a new path to develop high-performance OER electrocatalysts.

Keywords: cobalt ferrite; porous coatings; oxygen evolution reaction; water electrolysis catalysts; electrochemical impedance spectroscopy

check for updates

Citation: Kubisztal, J.; Kubisztal, M. Synthesis and Characterisation of Cobalt Ferrite Coatings for Oxygen Evolution Reaction. *Catalysts* **2022**, *12*, 21. https://doi.org/10.3390/catal12010021

Academic Editor: Carlo Santoro

Received: 2 December 2021
Accepted: 22 December 2021
Published: 25 December 2021

1. Introduction

The oxygen evolution reaction (OER) plays an essential role in state-of-art energy storage and conversion devices. Nowadays, the major challenge is to obtain low-cost and high-performance catalysts for those reactions. Electrodes made of Pt, IrO_2, and RuO_2 are known OER catalysts, however they are not appropriate for large-scale applications because of their cost. Transition metals, such as Fe, Ni, Co, and Mn, show high electrocatalytic activity and stability in alkaline solutions. Thus, they are promising candidates for replacing precious metals catalysts. Sulphides, selenides, nitrides, carbides, hydroxides, oxy-hydroxides, and oxides of transition metals are extensively used as efficient electrocatalysts [1–6]. Because of their high catalytic activity, relatively low cost, and environmental friendliness, numerous studies of transition metal oxides have been performed. For example, it has been found that NiO [7], Co_3O_4 [8], MnO_2 [9], and Fe_2O_3 [10] exhibit high catalytic activity toward OER compared to RuO_2 and IrO_2. It was also found that nickel- and cobalt- based composites usually produce overpotentials in the OER reaction around 350–450 mV at a current density of 10 $mAcm^{-2}$ [4–6].

Generally, spinel mixed metal oxides with formula AB_2O_4 (A, B = metal) exhibit higher electrochemical activity than the single-metal oxides. This is because of the electron jump among different valence states of ions in octahedral sites and additional metallic redox-active centres [11–16]. Between various spinel oxides, Fe-based spinels, e.g., $CuFe_2O_4$, $NiFe_2O_4$, and $CoFe_2O_4$, have been reported as promising electrocatalysts for OER [17]. However, the $CoFe_2O_4$ ferrite is one of the most interesting, especially for its excellent chemical stability, efficient electrocatalytic properties, high specific capacitance, low cost,

and environmental friendliness. Therefore, $CoFe_2O_4$ ferrite is a promising candidate as an electrode in water splitting, lithium-ion batteries, and supercapacitors [18–20]. Most of the mixed transition metal oxides catalysts are powders obtained by different methods, e.g., solvothermal, hydrothermal, electrodeposition, or spin coating [21,22]. Usually, to obtain an electrode, those powders are applied to a conductive substrate using a particle binder. However, polymeric binders are characterized by relatively poor electrical conductivity, which may influence the entire electrode's electrocatalytic activity. Additionally, the low durability of polymeric binders may also cause the detachment of coating that is especially noticeable at higher current densities and vigorous O_2 evolution [23]. Another frequently used method for electrode preparation is to anchor metal oxides on a carbon substrate. In this case, to assure sufficient functional groups, the carbon substrate is treated with harsh oxidative agents, which can deteriorate the electrical conductivity of the substrate and cause environmental pollution [24]. To improve the performance of these materials, various methods of their modifications have been reported, e.g., by creating nanoporous structures, synergistic metal–metal interactions, or embedding nanoparticles of catalysts in carbon nanomaterials [24–26]. However, there is still a need to design new MFe_2O_4 electrocatalysts with a very porous surface, high electrical conductivity, and durability.

This work has been carried out to study the electrocatalytic activity of the $CoFe_2O_4$ coatings during oxygen evolution reaction. Two different methods of electrode preparation have been used. In the first method, a coating consisting of a combination of $CoFe_2O_4$ powder and PEG 4000 (as a binder) was deposited by sedimentation on a metallic substrate. Subsequently, such prepared coating was subjected to heat treatment at 800 °C in an inert atmosphere. The second method used was the electrolytic co-deposition of nickel and $CoFe_2O_4$ powder. Electrodeposition seems to be an interesting alternative in coatings production that contain mixed metal oxides powders and metallic binders. Additionally, a nickel substrate subjected to the analogous treatment like $CoFe_2O_4$ coatings was also investigated.

2. Results and Discussion

2.1. $CoFe_2O_4$ Powder and Coating Characterization

The phase composition of the as-obtained and annealed (800 °C, 1 h, air) $CoFe_2O_4$ powder is shown in Figure 1. In both cases, X-ray diffraction patterns show the presence of the reflexes coming from the single-phase spinel cobalt ferrite with cubic crystal structure (space group: $Fd\bar{3}m$, lattice constant: a = 8.4101 Å, reference code: 04-009-8438 ICDD PDF4+ 2015). Note that XRD lines obtained for as-obtained $CoFe_2O_4$ particles are broadened due to some lattice strain [27]. The values of crystallite size calculated using the Williamson–Hall method [28] for as-obtained and annealed $CoFe_2O_4$ powders were 10(1) nm and 15(1) nm, respectively. Thus, one can state that $CoFe_2O_4$ powders are nanocrystalline phases and a 50% increase in the crystallite size is observed after annealing.

Figure 2 shows the SEM images of the examined samples, i.e., CFO_{PEG}, CFO_{Ni}, and $CFO_{Ni}^{a\text{-}r}$, and Ni substrate. One can see that the images obtained for CFO_{PEG} and CFO_{Ni} electrodes represent a relatively homogenous distribution of cobalt ferrite particles, while the image obtained for $CFO_{Ni}^{a\text{-}r}$ shows some agglomerates of $CoFe_2O_4$ particles separated from each other. Thus, heat treatment of $CoFe_2O_4$ powder (800 °C, 1 h, air) influences the shape of the electrode surface. Note that $CoFe_2O_4$ particles, independent of fabrication procedure applied, distinctly enlarge the surface roughness of the electrode in comparison with nickel substrate. The increased surface area should increase the electrocatalytic activity of the $CoFe_2O_4$ coatings towards oxygen evolution.

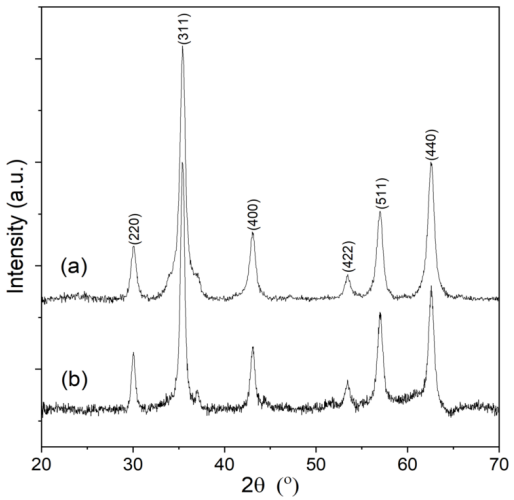

Figure 1. X-ray diffraction patterns of (**a**) as-received and (**b**) annealed at 800 °C for 1 h in the air $CoFe_2O_4$ powder.

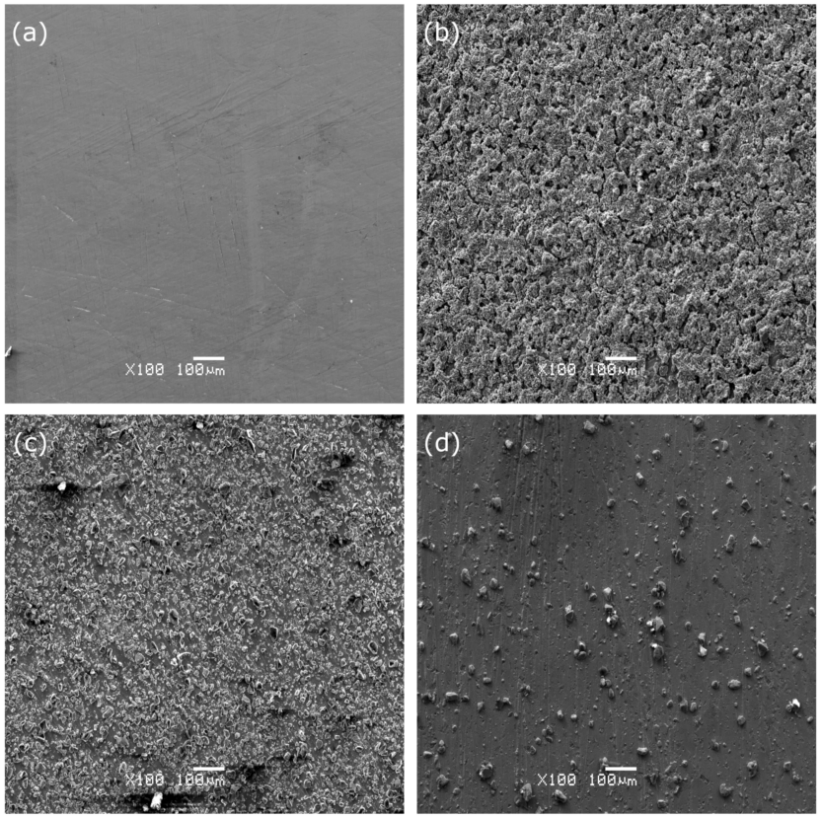

Figure 2. Surface morphology of (**a**) Ni substrate and (**b**) CFO_{PEG}, (**c**) CFO_{Ni}, (**d**) $CFO_{Ni}^{a\text{-}r}$ coatings.

2.2. Electrochemical Characterisation of $CoFe_2O_4$ Coatings

Investigations of the electrolytic oxygen evolution on the Ni and $CoFe_2O_4$ electrodes were carried out using *dc* and *ac* methods. In Figure 3a, quasi-stationary polarisation curves j vs. E are shown. It can be observed that the $CoFe_2O_4$ electrodes are more efficient than the Ni electrode. Among the $CoFe_2O_4$ electrodes, the lowest and the highest performance is observed for $CFO_{Ni}^{a\text{-}r}$ and CFO_{Ni} electrodes, respectively. For the linear part of polarisation curves, the Tafel equation $\eta = a + b\log|j|$ can be used to determine characteristic parameters of the electrode-electrolyte system. The parameters provide information about the mechanism (Tafel slope b) and the rate (apparent exchange current density j_0) of OER. It

can be seen from Figure 3b that all investigated electrodes show a well-defined Tafel region with a slope changing from 35 to 56 mVdec^{-1} (see also Table 1).

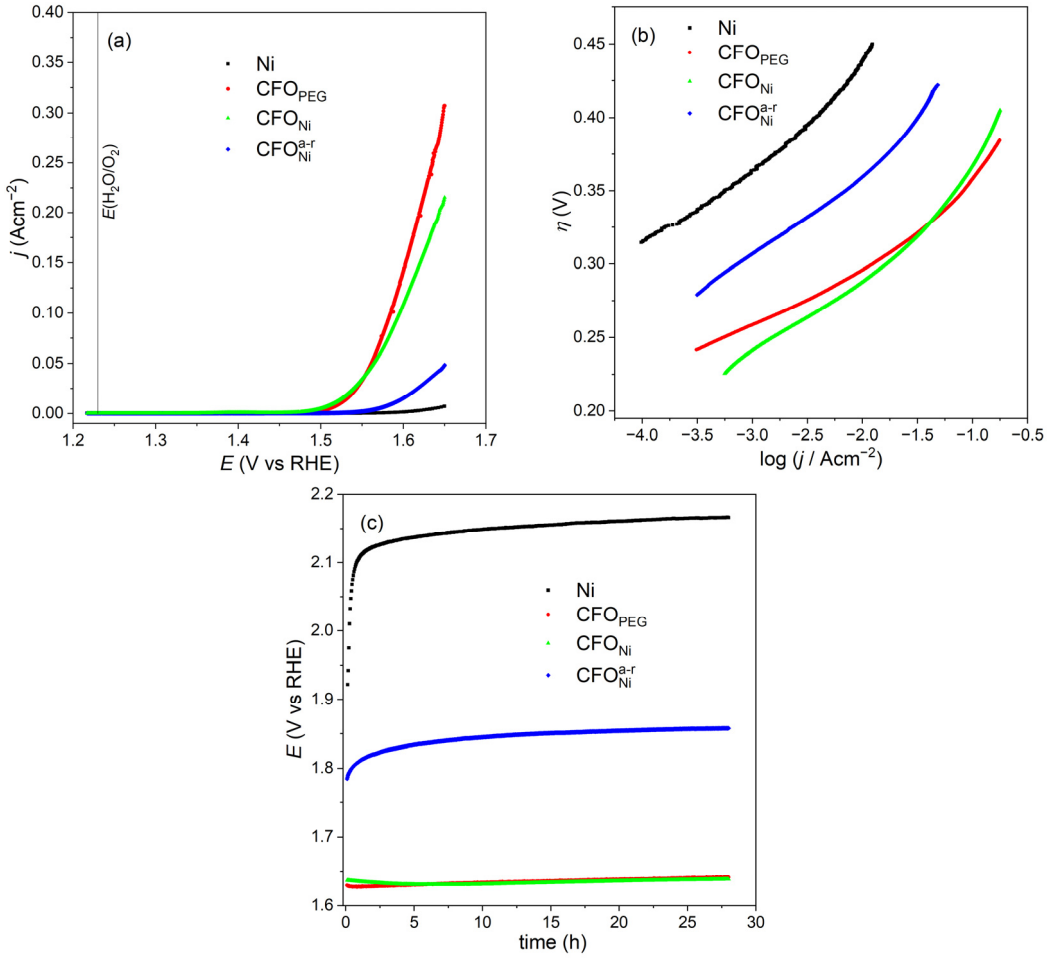

Figure 3. (**a**) polarisation curves, (**b**) Tafel plots and (**c**) chronopotentiometric curves obtained for $CoFe_2O_4$ electrodes in 1 M KOH.

Table 1. The Tafel slope b, the apparent exchange current density j_0, the overpotential at a current density of 10 mAcm^{-2} η_{10} and the average roughness factor $R_{f(av)}$ obtained for $CoFe_2O_4$ electrodes in 1 M KOH solution during OER.

	b (mVdec^{-1})	j_0 (Acm^{-2})	η_{10} (mV)	$R_{f(av)}$	$j_0/R_{f(av)}$ (Acm^{-2})
Ni	56	3.2×10^{-10}	438	12	2.7×10^{-11}
CFO$_{PEG}$	35	4.2×10^{-11}	295	1850	2.3×10^{-14}
CFO$_{Ni}$	45	4.6×10^{-9}	287	2487	1.8×10^{-12}
CFO$^{a-r}_{Ni}$	51	1.0×10^{-9}	359	93	1.1×10^{-11}

The OER mechanism consists of the following steps [29]:

$$M + OH^- \leftrightarrow MOH + e^-, \quad (1)$$

$$MOH + OH^- \leftrightarrow MO^- + H_2O, \quad (2)$$

$$MO^- \leftrightarrow MO + e^-, \quad (3)$$

$$2MO \leftrightarrow 2M + O_2. \quad (4)$$

Either (1) or (3) electrochemical reaction may be the rate-determining step (rds). When the surface coverage by OH is much smaller than one and the reaction (1) is rds, then the Tafel slope $b = 2.3RT/\beta F$. However, if the reaction (3) is rds, then $b = 2.3RT/(1 + \beta)F$ [29]. Assuming transfer coefficient $\beta = 0.5$ and temperature 25 °C, the theoretical Tafel slope for the reaction (1) is equal to 120 $mVdec^{-1}$ and for the reaction (3) 40 $mVdec^{-1}$. The Tafel slopes b obtained for all investigated $CoFe_2O_4$ coatings indicate that the OER proceeds via the same mechanism, with the third reaction step as the rate-determining step. The experimental b values higher than 40 $mVdec^{-1}$ indicate that the transfer coefficient is lower than 0.5. According to literature reports, it can be caused by anion adsorption and the nonuniform distribution of the surface electric field on the rough electrodes [29].

The parameter j_0 obtained for CFO_{Ni} and $CFO_{Ni}^{a\text{-}r}$ is ca. one order of magnitude higher in comparison with nickel electrode and ca. two orders of magnitude higher than for CFO_{PEG}. Such behaviour could be explained by the higher electrical conductivity of nickel ($\sigma \sim 10^6\ \Omega^{-1}cm^{-1}$) in comparison with cobalt ferrite particles ($\sigma \sim 10^{-7}\ \Omega^{-1}cm^{-1}$) [30]. Therefore, for CFO_{Ni} and $CFO_{Ni}^{a\text{-}r}$ electrodes, the electrolytically deposited nickel used as a particle binder causes an increase in the apparent exchange current density of the whole electrode.

The apparent activity of different electrodes could be compared using overpotential η determined at selected current density (in this work, $j = 10\ mAcm^{-2}$). For $CoFe_2O_4$ electrodes, the parameter η_{10} is from 80 mV to 150 mV lower in comparison with the nickel substrate (see Table 1). Thus, one can state that $CoFe_2O_4$ electrodes characterise higher apparent activity towards OER with respect to Ni electrode. It was also found that the apparent activity of CFO_{Ni} electrode modified by nickel binder is the highest among all investigated electrodes. For comparison, different kinds of $CoFe_2O_4$ electrodes reported in the literature for OER in alkaline media (1 M KOH or 1 M NaOH) are gathered in Table 2. All these data confirm that the CFO_{PEG}, CFO_{Ni}, and $CFO_{Ni}^{a\text{-}r}$ electrodes reveal high activity towards OER.

Table 2. Comparison of cobalt ferrite catalysts reported in the literature.

Catalyst	b ($mVdec^{-1}$)	η_{10} (mV)	Reference
$CoFe_2O_4$ (powders)	35	295	this work
$CoFe_2O_4$ (powders)	45	287	this work
$CoFe_2O_4$ (powders)	69	360	[12]
$CoFe_2O_4$ (powders)	126	435	[12]
$CoFe_2O_4$ (hollow nanofibers)	95	414	[11]
$CoFe_2O_4$ (thin films)	54	490	[13]
$CoFe_2O_4$ (nanoparticles)	73	378	[14]
$CoFe_2O_4$ (nanoplates)	61	360	[15]
$CoFe_2O_4$ (nanofibers)	107	340	[16]

In practical terms, an important criterion is the long-term stability of the catalysts. The stability of the cobalt ferrite electrodes in 1 M KOH solution was tested using the chronopotentiometry method at the constant current density of 50 $mAcm^{-2}$ (see Figure 3c). Percentage change of the measured potential determined for time period from 1 to 28 h is 5% for Ni, 3% for CFO_{PEG}, 1% for CFO_{Ni} and 7% for $CFO_{Ni}^{a\text{-}r}$. Thus, it can be stated that all investigated electrodes are relatively stable in an alkaline environment. Figure 4 shows the SEM images and corresponding maps of Ni, Fe, Co elements distribution for the CFO_{PEG} and CFO_{Ni} electrodes after 28 h of oxygen evolution. Comparison with images obtained before OER (Figure 2) indicates that the surface of CFO_{PEG} and CFO_{Ni} electrodes remained almost unchanged. Thus, SEM images confirm the conclusion obtained from electrochemical measurements. The distribution maps of elements indicate that the electrode surface consists of the porous coating made of $CoFe_2O_4$ particles (or their agglomerates) and nickel substrate in the case of CFO_{PEG} or nickel binder in the case of CFO_{Ni}.

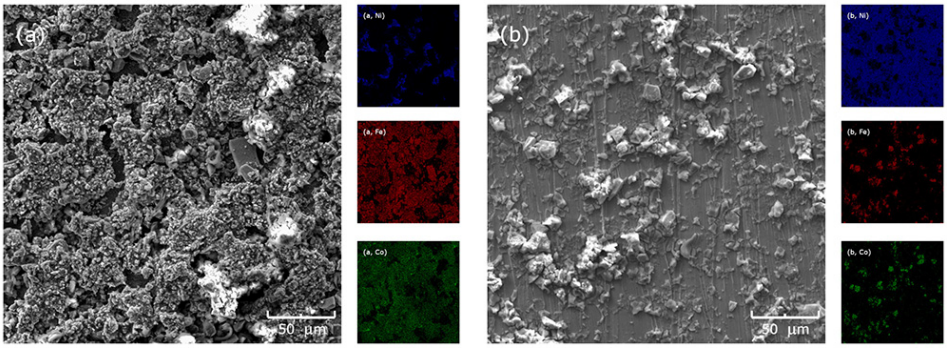

Figure 4. Surface morphology of (**a**) CFO_{PEG} and (**b**) CFO_{Ni} electrodes after 28 h of oxygen evolution at the current density j = 50 mAcm^{-2}.

Impedance spectra measured for selected potentials are shown in Figure 5. For all investigated electrodes, two semicircles on Nyquist plots are observed. There is a small potential-independent semicircle in the high-frequency region, and a potential-dependent semicircle in the low-frequency region. Such a shape of spectra is typical for porous electrodes. The potential-independent semicircle can be related to the geometry of the electrode surface, whereas the potential-dependent semicircle corresponds to the Faradaic reaction [31–33]. Thus, a model with two-time constants can adequately describe the response of porous $CoFeO_4$ electrodes during OER.

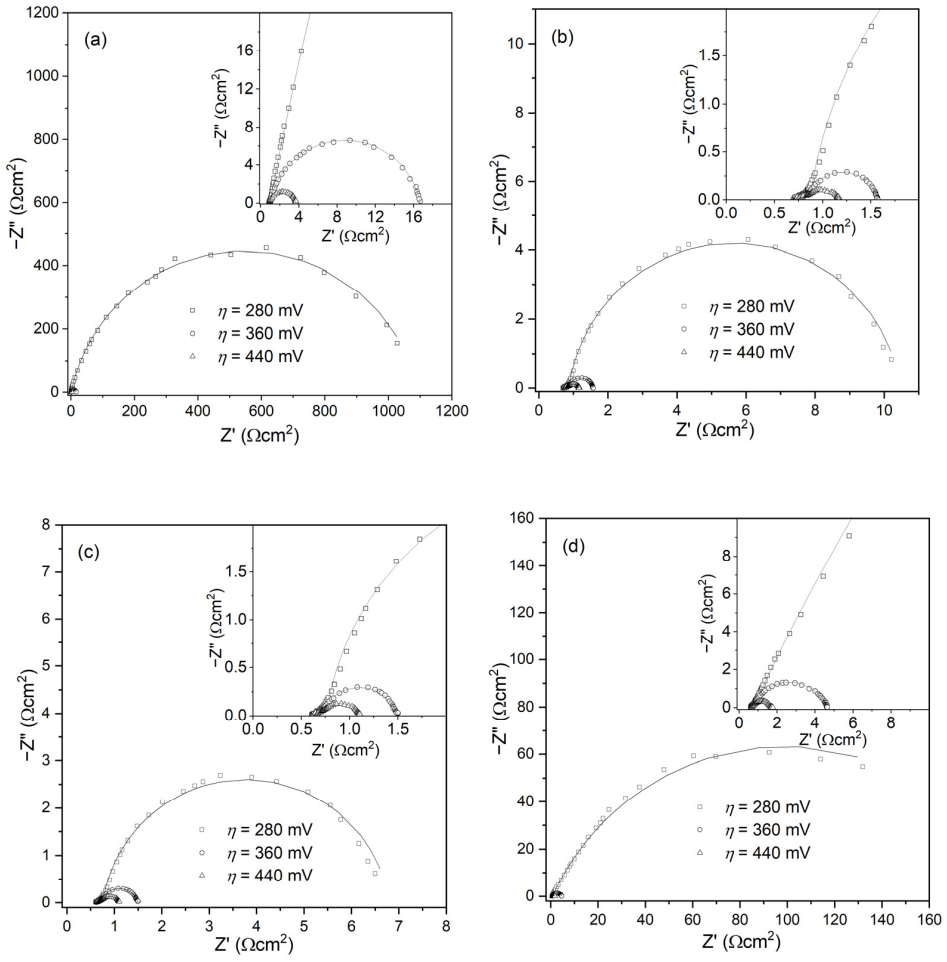

Figure 5. Complex impedance plots obtained for (**a**) Ni, (**b**) CFO_{PEG}, (**c**) CFO_{Ni} and (**d**) $CFO_{Ni}^{a\text{-}r}$ electrodes during the oxygen evolution process in 1 M KOH; symbols are experimental data, and lines were modelled using the electrical equivalent circuit shown in Figure 6.

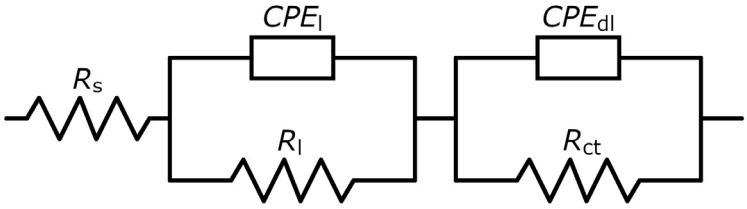

Figure 6. The electrical equivalent circuit used to describe oxygen evolution reaction on $CoFe_2O_4$ electrodes.

An electrical equivalent circuit used to describe the investigated process is shown in Figure 6. It contains solution resistance (R_s), coating capacitance ($CPE_{l.}$), coating resistance (R_l), charge transfer resistance (R_{ct}), and double layer capacitance (CPE_{dl}). Note that the deviation of solid electrodes from purely capacitive behaviour (caused by physical nonuniformity or uneven distribution of active sites) has been taken into account using *CPE* elements instead of capacitors. The following equation describes the impedance of the *CPE* element: $Z_{CPE} = 1/T(j\omega)^{\phi}$, where T is the capacity parameter and ϕ is the dispersion parameter related to the depression angle [31–33].

For all obtained electrodes, the value of charge transfer resistance decreases with increasing overpotential, which corresponds to the decreasing diameter of the low-frequency semicircle (see Figure 5). Furthermore, comparing R_{ct} with the R_l, it was found that $R_{ct} >> R_l$. Thus, R_{ct} governs the electrode kinetic. The relation η vs. $\log(R_{ct}{}^{-1})$ for all investigated electrodes is shown in Figure 7. It was found that R_{ct} values obtained for $CoFe_2O_4$ at lower overpotentials can be over 100 times lower than that obtained for Ni electrode and in both cases gradually decreases with increasing overpotential. Additionally, η vs. $\log(R_{ct}{}^{-1})$ curves show well-defined linear regions with slopes from 40 to 48 $mVdec^{-1}$. Note that the obtained slopes correlate with Tafel coefficients obtained from η vs. $\log(j)$ curves.

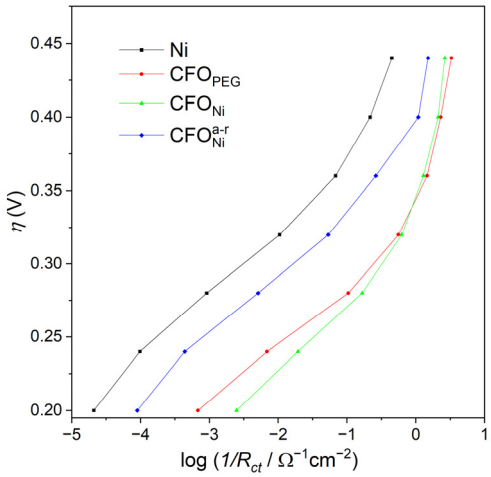

Figure 7. Overpotential η versus $\log 1/R_{ct}$ obtained for $CoFe_2O_4$ electrodes in 1 M KOH during the oxygen evolution process.

The double layer capacitance C_{dl} can be determined using the equation: $C_{dl} = [T/((R_s + R_l)^{-1} + R_{ct}{}^{-1})^{(1-\phi)}]^{1/\phi}$ [32]. The relation between C_{dl} and η for all obtained coatings is shown in Figure 8. It was found that the smallest value of C_{dl} was obtained for the nickel electrode, as should be expected. CFO_{Ni} and CFO_{PEG} coatings exhibit, respectively, ca. 200 times and ca. 150 times higher C_{dl} (average value) in comparison with nickel electrode.

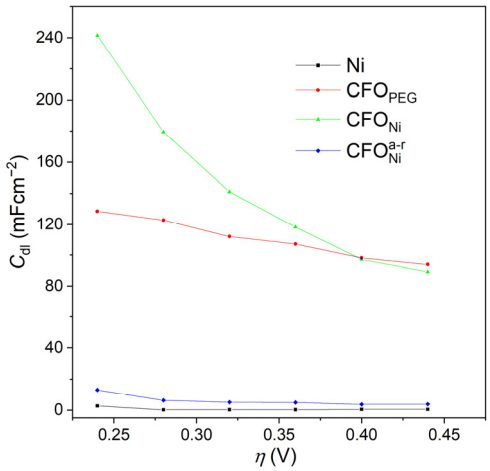

Figure 8. Double layer capacitance C_{dl} versus overpotential η obtained for $CoFe_2O_4$ electrodes in 1 M KOH during the oxygen evolution process.

Note that double layer capacitance is directly proportional to the electrochemically accessible surface area. Assuming that the double layer capacitance of the smooth oxide surface is 60 μFcm^{-2} [29,33], the roughness factor R_f can be calculated as $R_f = C_{dl}/60$ μFcm^{-2}. The intrinsic exchange current density (calculated as j_0/R_f) indicates that the superior catalytic properties of CFO_{PEG} electrode are mainly the result of the large electrochemically accessible surface area. In turn, the excellent CFO_{Ni} electrode properties result from both high intrinsic catalytic activity and large electrochemically accessible surface area. Note that the most useful case for the electrocatalysis is when the whole area of an electrode is accessible to reactants. As can be seen in Figure 8, the double layer capacitance obtained for all electrodes decreases with increasing overpotential. This may result from the fact that oxygen bubbles partially block the electrode surface. However, it should be emphasized that even at high overpotentials, CFO_{PEG} and CFO_{Ni} electrodes are characterized by much higher values of C_{dl} compared to the nickel substrate.

3. Materials and Methods

3.1. Cobalt Ferrite Powder Synthesis

The $CoFe_2O_4$ powder was synthesised using the coprecipitation method [27] and reagents of analytical purity (POCh, Gliwice, Poland). Hence, 0.6 moldm^{-3} of $FeCl_3 \cdot 6H_2O$ and 0.3 moldm^{-3} of $CoCl_2 \cdot 6H_2O$ solutions were mixed in ultrapure water with a resistivity of 18.2 MΩcm. Precipitating agent, i.e., NaOH (2 moldm^{-3}), was slowly added to the stirred chlorides solution. Coprecipitation was conducted in a Teflon vessel at a temperature of 50 °C for two hours. Subsequently, the synthesised powder was rinsed in distilled water, centrifuged for five minutes at 300 rpm, and dried at 50 °C for 48 h. The powder was also ground in an agate mortar to break agglomerates into smaller particles. In further study, the as-received and post-thermal treatment (800 °C, 1 h, air) $CoFe_2O_4$ powder was used. The phase composition of $CoFe_2O_4$ powder was determined by X-ray diffraction technique (XRD) using a Philips X'Pert PW 3040/60 diffractometer (PANalytical, Almelo, Netherlands) equipped with $Cu_{K\alpha}$ radiation. The ICDD cards were used for phase identification.

3.2. Preparation of Cobalt Ferrite Coatings

Cobalt ferrite coatings were deposited on a nickel plate (Nickel 201, Ni ≥ 99.0%). Before the deposition process, the nickel plate with a working area of 0.5 cm^2 was mechanically polished using abrasive papers (P320, P600, P1000), and subsequently rinsed in acetone in an ultrasonic bath for 10 min. The studied coatings were produced by applying two different procedures. In the first case, a mixture of the thermally treated $CoFe_2O_4$ powder (20 mg per 10 mL of solution) and polyethylene glycol 4000 (PEG 4000) (20 mg per 10 mL of solution) in acetone was prepared. Additionally, 5 mg of sodium dodecyl

sulfate (SDS) was added as a surfactant to the mixture. To obtain a homogeneous colloid, the prepared mixture was placed in an ultrasonic bath for 30 min. Subsequently, the nickel substrate was immersed in the mixture. The coating was deposited by sedimentation on a metallic substrate until all the solvent had evaporated. The obtained coating was subjected to heat treatment at 800 °C for 1 h in an argon atmosphere. In this paper, coating obtained in that way will be referred to as CFO_{PEG}. In the second case, to obtain $CoFe_2O_4$ coating with a metallic binder, electrochemical deposition was used. Nickel was deposited from the bath with the following composition (concentrations in gdm^{-3}): $NiSO_4 \cdot 7H_2O$—84, $NiCl_2 \cdot 6H_2O$—10, H_3BO_3—8, to which 20 mg of cobalt ferrite powder and 5 mg of SDS was added. Note that nickel electrodeposition started when $CoFe_2O_4$ powder settled by sedimentation on the surface of the metallic substrate. Nickel binder was deposited under galvanostatic conditions at current density $j = 10$ $mAcm^{-2}$ and time 20 min. The deposition process was carried out at the temperature 20 °C. The Faradaic yield of nickel deposition was ca. 70%. In this paper, coatings obtained in that way will be referred to as CFO_{Ni} (in the case of thermally treated $CoFe_2O_4$ powder) and $CFO_{Ni}^{a\text{-}r}$ (in the case of as-received $CoFe_2O_4$ powder). Using a JEOL JSM—6480 (JEOL Ltd., Tokyo, Japan) scanning electron microscope (SEM) with energy dispersive spectroscopy (EDS) attachment, the surface morphology and chemical composition of the obtained $CoFe_2O_4$ coatings were determined.

3.3. Electrochemical Measurements

Electrochemical tests were performed in 1 M KOH solution using a three-electrode cell with saturated calomel electrode (SCE) as a reference electrode and platinum mesh as a counter electrode. Working electrodes were $CoFe_2O_4$ coatings with a geometric surface area of 0.5 cm^2. The ohmic drop between the reference and working electrode was reduced using a Luggin capillary. All electrochemical experiments were carried out at a temperature of 20 °C. For the data registration, a PARSTAT 2273 system and the PowerSuite 2.58 software (Princeton Applied Research, Oak Ridge, TN, USA) were used. Values of measured potentials were converted from SCE to reversible hydrogen electrode (RHE) according to the following formula: $E_{RHE} = E_{SCE} + 0.059pH + 0.241$. The overpotential ($\eta$) for the oxygen evolution reaction was calculated using the equation: $\eta = E_{RHE} - 1.23$.

Quasi-stationary polarisation curves j vs. E were recorded using the linear sweep voltammetry (LSV) technique within the potential range from 1.22 V to 1.85 V vs. RHE and sweep rate $v = 10$ $mVmin^{-1}$. Before measurements, $CoFe_2O_4$ electrodes were conditioned at an anodic potential of 1.85 V for 5 h. The ohmic drop compensation was conducted during measurements using the current interrupt technique [4].

The spectra were registered using the electrochemical impedance spectroscopy (EIS) method. The impedance spectra were recorded potentiostatically at selected *dc* potentials from the interval where the OER takes place. Before the recording of each spectrum, electrodes were held at the appropriate potential for 5 min. Spectra were registered in the frequency range from 20 kHz to 10 mHz with a density of 10 points per decade. The amplitude of the *ac* signal was 10 mV_{rms}. For the quantitative analysis of obtained data, the ZSimpWin 3.21 software was used.

To evaluate long-term stability of the $CoFe_2O_4$ electrodes, the chronopotentiometry technique was used. The test was carried out at the current density $j = 50$ $mAcm^{-2}$ for 28 h.

4. Concluding Remarks

This paper reports on two new procedures for the preparation of porous cobalt ferrite coatings with a metallic and organic binder for use as catalysts in the oxygen evolution reaction (OER). The parameter η_{10} indicates that all investigated $CoFe_2O_4$ coatings exhibit significantly higher apparent activity towards OER than nickel substrate in 1 M KOH. In particular, $CoFe_2O_4$ coating with PEG applied as a binder shows overpotential $\eta_{10} = 295$ mV at a current density of 10 $mAcm^{-2}$ and Tafel slope $b = 35$ $mVdec^{-1}$. $CoFe_2O_4$ coating with Ni binder ($\eta_{10} = 287$ mV and $b = 45$ $mVdec^{-1}$) shows comparable catalytic activity towards OER. It was stated that the main reason for the superior catalytic activity of CFO_{PEG} coating

is the large electrochemically active surface area. In contrast, the excellent catalytic activity of $CoFe_2O_4$ coating containing nickel binder between the ferrite particles is caused by increasing both the conductivity and the electrochemically active surface area. It was also shown that the obtained $CoFe_2O_4$ electrodes maintain their catalytic activity for at least 28 h at a current density of 50 $mAcm^{-2}$. It can be stated that this work offers a new path for the design of high-performance OER electrocatalysts using both sintering and electrodeposition techniques.

Author Contributions: Conceptualization, J.K. and M.K.; methodology, J.K. and M.K.; formal analysis, J.K. and M.K.; investigation, J.K. and M.K.; writing—original draft preparation, J.K.; writing—review and editing, J.K. and M.K.; visualization, J.K.; funding acquisition, J.K. All authors have read and agreed to the published version of the manuscript.

Funding: Publication co-financed by the funds granted under the Research Excellence Initiative of the University of Silesia in Katowice.

Institutional Review Board Statement: Not applicable.

Informed Consent Statement: Not applicable.

Data Availability Statement: The data presented in this study are available on request from the corresponding author.

Acknowledgments: The authors wish to express their gratitude to Jan Rak (University of Silesia in Katowice, Poland) for technical support with SEM/EDS measurements.

Conflicts of Interest: The authors declare no conflict of interest.

References

1. Hu, X.; Tian, X.; Lin, Y.-W.; Wang, Z. Nickel foam and stainless steel mesh as electrocatalysts for hydrogen evolution reaction, oxygen evolution reaction and overall water splitting in alkaline media. *RSC Adv.* **2019**, *9*, 31563–31571. [CrossRef]
2. Aziz, A.; Asif, M.; Ashraf, G.; Iftikhar, T.; Hu, J.; Xiao, F.; Wang, S. Boosting electrocatalytic activity of carbon fiber@fusiform-like copper-nickel LDHs: Sensing of nitrate as biomarker for NOB detection. *J. Hazard. Mater.* **2022**, *422*, 126907. [CrossRef] [PubMed]
3. Asif, M.; Aziz, A.; Ashraf, G.; Iftikhar, T.; Sun, Y.; Xiao, F.; Liu, H. Unveiling microbiologically influenced corrosion engineering to transfigure damages into benefits: A textile sensor for H_2O_2 detection in clinical cancer tissues. *Chem. Eng. J.* **2022**, *427*, 131398. [CrossRef]
4. Colli, A.N.; Girault, H.H.; Battistel, A. Non-precious electrodes for practical alkaline water electrolysis. *Materials* **2019**, *12*, 1336. [CrossRef] [PubMed]
5. Chen, F.; Zhang, L.L.; Wu, H.; Guan, C.; Yang, Y.; Qiu, J.; Lyu, P.; Li, M. Bifunctional oxygen evolution and supercapacitor electrode with integrated architecture of NiFe-layered double hydroxides and hierarchical carbon framework. *Nanotechnology* **2019**, *30*, 325402. [CrossRef]
6. Wang, Y.; Qiao, M.; Li, Y.; Wang, S. Tuning surface electronic configuration of NiFe LDHs nanosheets by introducing cation vacancies (Fe or Ni) as highly efficient electrocatalysts for oxygen evolution reaction. *Small* **2018**, *14*, 1800136. [CrossRef] [PubMed]
7. Nardi, K.L.; Yang, N.Y.; Dickens, C.F.; Strickler, A.L.; Bent, S.F. Creating highly active atomic layer deposited NiO electrocatalysts for the oxygen evolution reaction. *Adv. Energy Mater.* **2015**, *5*, 1500412. [CrossRef]
8. Zhu, X.L.; Wang, P.; Wang, Z.Y.; Liu, Y.Y.; Zheng, Z.K.; Zhang, Q.Q.; Zhang, X.Y.; Dai, Y.; Whangbo, M.H.; Huang, B.B. Co_3O_4 nanobelt arrays assembled with ultrathin nanosheets as highly efficient and stable electrocatalysts for the chlorine evolution reaction. *J. Mater. Chem. A* **2018**, *6*, 12718–12723. [CrossRef]
9. Meng, Y.T.; Song, W.Q.; Huang, H.; Ren, Z.; Chen, S.Y.; Suib, S.L. Structure–property relationship of bifunctional MnO_2 nanostructures: Highly efficient, ultra-stable electrochemical water oxidation and oxygen reduction reaction catalysts identified in alkaline media. *J. Am. Chem. Soc.* **2014**, *136*, 11452–11464. [CrossRef] [PubMed]
10. Jung, J.W.; Jang, J.S.; Yun, T.G.; Yoon, K.R.; Kim, I.D. Three-dimensional nanofibrous air electrode assembled with carbon nanotubes-bridged hollow Fe_2O_3 nanoparticles for high-performance lithium-oxygen batteries. *ACS Appl. Mater. Interfaces* **2018**, *10*, 6531–6540. [CrossRef]
11. Silva, V.D.; Ferreira, L.S.; Simoes, T.A.; Medeiros, E.S.; Macedo, D.A. 1D hollow MFe_2O_4 (M = Cu, Co, Ni) fibers by solution blow spinning for oxygen evolution reaction. *J. Colloid Interface Sci.* **2019**, *540*, 59–65. [CrossRef]
12. Ferreira, L.S.; Silva, T.R.; Santos, J.R.D.; Silva, V.D.; Raimundo, R.A.; Morales, M.A.; Macedo, D.A. Structure, magnetic behavior and OER activity of $CoFe_2O_4$ powders obtained using agar-agar from red seaweed (Rhodophyta). *Mater. Chem. Phys.* **2019**, *237*, 121847. [CrossRef]
13. Sagu, J.S.; Mehta, D.; Wijayantha, K.G.U. Electrocatalytic activity of $CoFe_2O_4$ thin films prepared by AACVD towards the oxygen evolution reaction in alkaline media. *Electrochem. Commun.* **2018**, *87*, 1–4. [CrossRef]

14. Kargar, A.; Yavuz, S.; Kim, T.K.; Liu, C.-H.; Kuru, C.; Rustomji, C.S.; Jin, S.; Bandaru, P.R. Solution-processed $CoFe_2O_4$ nanoparticles on 3D carbon fiber papers for durable oxygen evolution reaction. *ACS Appl. Mater. Interfaces* **2015**, *7*, 17851–17856. [CrossRef]
15. Mahala, C.; Sharma, M.D.; Basu, M. 2D nanostructures of $CoFe_2O_4$ and $NiFe_2O_4$: Efficient oxygen evolution catalyst. *Electrochim. Acta* **2018**, *273*, 462–473. [CrossRef]
16. Zhang, Z.; Zhang, J.; Wang, T.; Li, Z.; Yang, G.; Bian, H.; Li, J.; Gao, D. Durable oxygen evolution reaction of one dimensional spinel $CoFe_2O_4$ nanofibers fabricated by electrospinning. *RSC Adv.* **2018**, *8*, 5338–5343. [CrossRef]
17. Li, M.; Xiong, Y.P.; Liu, X.T.; Bo, X.J.; Zhang, Y.F.; Han, C.; Guo, L.P. Facile synthesis of electrospun MFe_2O_4 (M = Co, Ni, Cu, Mn) spinel nanofibers with excellent electrocatalytic properties for oxygen evolution and hydrogen peroxide reduction. *Nanoscale* **2015**, *7*, 8920–8930. [CrossRef]
18. Karthigayan, N.; Manimuthu, P.; Priya, M.; Sagadevan, S. Synthesis and characterisation of $NiFe_2O_4$, $CoFe_2O_4$ and $CuFe_2O_4$ thin films for anode material in Li-ion batteries. *Nanomater. Nanotechnol.* **2017**, *7*, 1847980417711084. [CrossRef]
19. Nikam, S.M.; Sharma, A.; Rahaman, M.; Teli, A.M.; Mujawar, S.H.; Zahn, D.R.T.; Patil, P.S.; Sahoo, S.C.; Salvan, G.; Patil, P.B. Pulsed laser deposited $CoFe_2O_4$ thin films as supercapacitor electrodes. *RSC Adv.* **2020**, *10*, 19353–19359. [CrossRef]
20. Zhang, L.H.; Wei, T.; Jiang, Z.M.; Liu, C.Q.; Jiang, H.; Chang, J.; Sheng, L.Z.; Zhou, Q.H.; Yuan, L.B.; Fan, Z.J. Electrostatic interaction in electrospun nanofibers: Double-layer carbon protection of $CoFe_2O_4$ nanosheets enabling ultralong-life and ultrahigh-rate lithium ion storage. *Nano Energy* **2018**, *48*, 238–247. [CrossRef]
21. Richter, P.; Plassmeyer, P.N.; Harzdorf, J.; Ruffer, T.; Lang, H.; Kalbacova, J.; Johrmann, N.; Schulze, S.; Hietschold, M.; Arekapudi, S.S.P.K.; et al. High quality magnetic oxide thin films prepared via aqueous solution processing. *Chem. Mater.* **2016**, *28*, 4917–4927. [CrossRef]
22. Kennaz, H.; Harat, A.; Guellati, O.; Momodu, D.Y.; Barzegar, F.; Dangbegnon, J.K.; Manyala, N.; Guerioune, M. Synthesis and electrochemical investigation of spinel cobalt ferrite magnetic nanoparticles for supercapacitor application. *J. Solid State Electrochem.* **2018**, *22*, 835–847. [CrossRef]
23. Lu, X.; Zhao, C. Electrodeposition of hierarchically structured three-dimensional nickel–iron electrodes for efficient oxygen evolution at high current densities. *Nat. Commun.* **2015**, *6*, 6616. [CrossRef] [PubMed]
24. Liang, Y.; Li, Y.; Wang, H.; Dai, H. Strongly coupled inorganic/nanocarbon hybrid materials for advanced electrocatalysis. *J. Am. Chem. Soc.* **2013**, *135*, 2013–2036. [CrossRef] [PubMed]
25. Liang, Y.; Li, Y.; Wang, H.; Zhou, J.; Wang, J.; Regier, T.; Dai, H. Co_3O_4 nanocrystals on graphene as a synergistic catalyst for oxygen reduction reaction. *Nat. Mater.* **2011**, *10*, 780–786. [CrossRef]
26. Gong, M.; Li, Y.; Wang, H.; Liang, Y.; Wu, J.Z.; Zhou, J.; Wang, J.; Regier, T.; Wei, F.; Dai, H. An advanced Ni-Fe layered double hydroxide electrocatalyst for water oxidation. *J. Am. Chem. Soc.* **2013**, *135*, 8452–8455. [CrossRef]
27. Kubisztal, M.; Kubisztal, J.; Karolus, M.; Prusik, K.; Haneczok, G. Collective superspin glass state of interacting cobalt ferrite nanoparticles. *IEEE Trans. Magn.* **2019**, *55*, 2301306. [CrossRef]
28. Williamson, G.K.; Hall, W.H. X-ray line broadening from filed aluminium and wolfram. *Acta. Metall.* **1953**, *1*, 22–31. [CrossRef]
29. Yan, Z.; Liu, H.; Hao, Z.; Yu, M.; Chen, X.; Chen, J. Electrodeposition of (hydro)oxides for an oxygen evolution electrode. *Chem. Sci.* **2020**, *11*, 10614–10625. [CrossRef]
30. Ajroudi, L.; Mliki, N.; Bessais, L.; Madigou, V.; Villain, S.; Leroux, C. Magnetic, electric and thermal properties of cobalt ferrite nanoparticles. *Mater. Res. Bull.* **2014**, *59*, 49–58. [CrossRef]
31. Lasia, A. *Electrochemical Impedance Spectroscopy and Its Applications*, 1st ed.; Springer: New York, NY, USA, 2014; pp. 203–250. [CrossRef]
32. Kubisztal, J.; Budniok, A.; Lasia, A. Study of the hydrogen evolution reaction on nickel-based composite coatings containing molybdenum powder. *Int. J. Hydrogen Energy* **2007**, *32*, 1211–1218. [CrossRef]
33. Louie, M.W.; Bell, A.T. An investigation of thin-film Ni-Fe oxide catalysts for the electrochemical evolution of oxygen. *J. Am. Chem. Soc.* **2013**, *135*, 12329–12337. [CrossRef] [PubMed]